

Experimental characterization of entanglement dynamics in noisy channels

Jin-Shi Xu, Chuan-Feng Li*, Xiao-Ye Xu, Cheng-Hao Shi, Xu-Bo Zou, and Guang-Can Guo

*Key Laboratory of Quantum Information,
University of Science and Technology of China,
CAS, Hefei, 230026, People's Republic of China*

(Dated: December 7, 2018)

Abstract

The dynamics of entanglement between two photons with one of them passing through noisy quantum channels is characterized. It is described by a simple factorization law which was first theoretically proposed by Konrad *et al.* [Nature Phys., 4, 99 (2008)]. Quantum state tomography process is employed to reconstruct the reduced density matrixes of the final states and the corresponding concurrences are calculated. Good fittings between experimental results and theoretical predictions are found, which imply the validity of the general factorization law in the characterization of entanglement dynamics.

PACS numbers: 03.67.Mn, 03.65.Yz, 03.65.Ud

* email: cfl@ustc.edu.cn

Entanglement is the crucial resource for quantum communication and computation [1]. However, due to unavoidable couplings with the environment, it is readily destroyed when entangled particles transmitted through noisy quantum channels [2]. Characterization the dynamics of entanglement becomes an important task for those entanglement-based quantum information processing protocols and it is also crucial for understanding the distinct properties of entanglement dynamics, such as the phenomenon of entanglement sudden death [3, 4, 5, 6, 7].

In order to quantify the entanglement, we need a convenient quantity to measure it. The Woottter's concurrence [8] is a good choice for two qubits, which is given by

$$C = \max\{0, \Gamma\}, \quad (1)$$

where $\Gamma = \sqrt{\lambda_1} - \sqrt{\lambda_2} - \sqrt{\lambda_3} - \sqrt{\lambda_4}$ and the λ_i are the eigenvalues in decreasing order of the matrix $\rho(\sigma_y \otimes \sigma_y)\rho^*(\sigma_y \otimes \sigma_y)$. σ_y is the second Pauli matrix and ρ^* is the complex conjugate of ρ in the canonical basis $\{|00\rangle, |01\rangle, |10\rangle, |11\rangle\}$. The concurrence ranges from 0 (the separated state) to 1 (the maximally entangled state).

Usually, the tomography process [9] which requires measurement on a complete set of observable quantities is used to reconstruct the final density matrix ρ and the entanglement of the state is always nonlinear dependent on it [10], just as we have shown above. Therefore, the knowledge of the dynamics of entanglement can only deduce from the time evolution of the state [3, 4, 5, 7, 11, 12, 13, 14]. The general result on entanglement dynamics is still a great challenge.

Recently, the work of Konrad *et al.* gives a general factorization law on the entanglement dynamics of the biparticle system under the action of an arbitrary channel on one of the component [15]. The main result they got is the formulation:

$$C[(\mathbf{1} \otimes \$)|\chi\rangle\langle\chi|] = C[(\mathbf{1} \otimes \$)|\phi^+\rangle\langle\phi^+|]C(|\chi\rangle), \quad (2)$$

where $|\chi\rangle$ is the initial input pure state and $|\phi^+\rangle$ is the maximally entangled state. We use C_{LP} to represent the left term of the equality and C_{RP} to represent the right term, for simplicity. It is clearly shown that the entanglement dynamics in the one-sided noisy channel only relate to the dynamics of the maximally entangled state in the channel with a factor of the concurrence of the initial state $|\chi\rangle$.

Due to the convexity property of concurrence [8], this factorization law can be generalized

to the mixed initial state ρ_0 [15]

$$C[(\mathbb{1} \otimes \$)\rho_0] \leq C[(\mathbb{1} \otimes \$)|\phi^+\rangle\langle\phi^+|]C(\rho_0). \quad (3)$$

We also use C_{LM} and C_{RM} to represent the left and the right terms of this inequality, respectively. This inequality gives the upper bound of the evolved entanglement.

Here, using an all optical setup, we experimentally characterize the two-photon entanglement dynamics with one of the photons passing through the phase damping channel or the amplitude decay channel. The experimental results show that the time evolution of entanglement is fully characterized by the channel's action on the maximally entangled state and we verify the factorization laws.

Our experimental setup is shown in Figure 1. Ultraviolet (UV) pulses with wavelength centered at 390 nm which are frequency doubled from a Ti:sapphire laser with a pulse width of 130 fs and a repetition rate of 76 MHz pump into a two geometry type I beta-barium-borate (BBO) crystals to generate entangled two photons [16]. The polarization of these UV pulses is set by the half-wave plate HWP0 which can be used to prepared different pure input states $|\chi\rangle = \alpha|HH\rangle_{a,b} + \beta|VV\rangle_{a,b}$ (α and β are the relative amplitudes which are set to be real for simplicity and they obey the relationship of $\alpha^2 + \beta^2 = 1$). Quartz plates (CP) in both emitted modes a and b are used to compensate the temporal difference between horizontal and vertical polarization components in these two nonlinear crystals [17].

A Fabry-Perot (F-P) cavity followed by quartz plates Q2 in the dotted pane M is used to simulate the phase damping channel, which has been used in our previous experiment [7]. When the photon passes through Q2 with thickness L , the relative phase between H - and V -polarization photon can be calculated as $\phi = L\Delta n\omega/c$, where c is the velocity of the photon in the vacuum. $\Delta n = n_o - n_e$ is the difference between the indexes of refraction of ordinary light (n_o) and extraordinary light (n_e), which can be treated as a constant of 0.01 for the small frequency distribution. The amplitude decay channel shown also in the dotted pane M is simulated by a sets of glass slabs (gs) which are tilted to the Brewster angles (about 57°) [18]. After passing through the slaps, the photon with vertical polarization has some probability to reflect and the photon with horizontal polarization will transmit completely. Therefore, the corresponding quantum map [19] can be written as

$$\begin{aligned} |H\rangle_S|0\rangle_E &\longrightarrow |H\rangle_S|0\rangle_E, \\ |V\rangle_S|0\rangle_E &\longrightarrow \sqrt{1-\epsilon}|V\rangle_S|0\rangle_E + \sqrt{\epsilon}|H\rangle_S|1\rangle_E. \end{aligned} \quad (4)$$

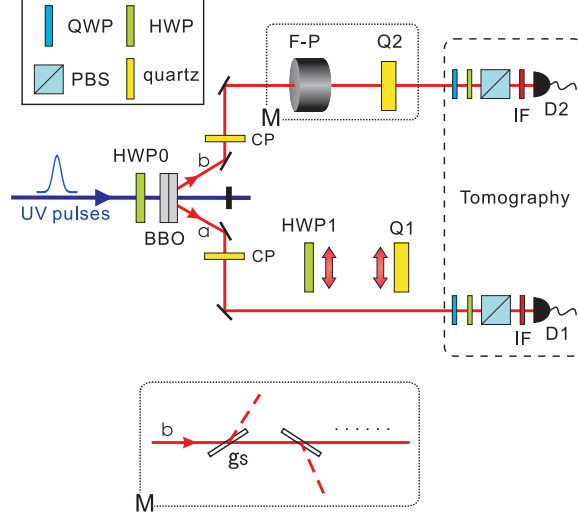


FIG. 1: (Color online). The experimental setup to investigate the entanglement dynamics in different noisy channels. Entangled polarization photon pairs generated from the adjacent nonlinear crystals (BBO) emit into modes a and b . The half-wave plate (HWP0) is used to change the polarization of the pump light. A half-wave plate (HWP1) and quartz plates (Q1) are inserted into mode a depending on different cases. The dotted pane M represents the noisy channels. The Fabry-Perot (F-P) cavity followed by quartz plates (Q2) simulates the phase damping channel, while the sets of glass slabs (gs) which are tilted to the Brewster angles represent the amplitude decay channels (the dashed lines represent the reflected photons). Quarter-wave plates (QWP), half-wave plates (HWP) and polarization beam splitters (PBS) in both arms are used to set the detecting polarization bases for the state reconstruction. Both photons are finally detected by silicon avalanche photodiodes (D1 and D2) equipped with 3 nm interference filters to give coincident counts.

where $|0\rangle_E$ and $|1\rangle_E$ represent the propagation paths of the photon and ϵ represents the total reflectivity of the glass slaps. We can change the polarization of the reflected photon into $|H\rangle$ with half-wave plates and detect them with single photon detectors (not shown in fig. 1).

A half-wave plate (HWP1) and quartz plates (Q1) are inserted into mode a depending on different cases to introduce different decoherence effect on the maximally entangled state $|\phi^+\rangle = \frac{1}{\sqrt{2}}(|HH\rangle_{a,b} + |VV\rangle_{a,b})$ to prepare different mixed input states. The optical axis of HWP1 is set to be 22.5° operating as a Hadamard gate and Q1 with the optical axis set to

be horizontal can induce relative phase in the basis H/V .

The density matrixes of the final states are reconstructed by the tomography process [9]. Experimentally, quarter-wave plates (QWP), half-wave plates (HWP) and polarization beam splitters (PBS) in both arms are used to set the standard 16 polarization analysis measurement bases [9]. Both photons are detected by silicon avalanche photodiodes D1 and D2 to give coincident counts. Narrow band interference filters (IF) with a full width at half maximum (FWHM) of 3 nm in front of detectors are used to reduce the background and define the bandwidth of the photons.

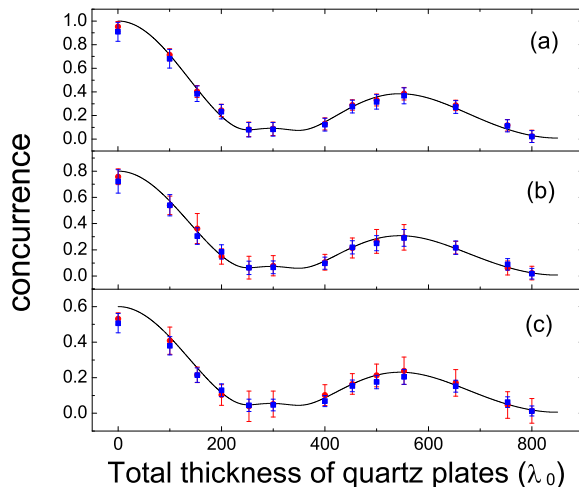


FIG. 2: (Color online). Experimental results for the entanglement dynamics of different pure initial states in the phase-damping channel. (a) $\alpha^2 = \frac{1}{2}$. (b) $\alpha^2 = \frac{1}{5}$. (c) $\alpha^2 = \frac{1}{10}$. Red dots and blue squares represent C_{LP} and C_{RP} , respectively. The solid lines and dashed lines representing the theoretical predictions of C_{LP} and C_{RP} completely overlap. $\lambda_0=780$ nm.

We first demonstrate the entanglement dynamics of different pure input states in the phase-damping channel, as shown in fig. 2. Three different pure input states $|\chi\rangle$ with $\alpha^2 = \frac{1}{2}$ (fig. 2(a)), $\alpha^2 = \frac{1}{5}$ (fig. 2(b)), $\alpha^2 = \frac{1}{10}$ (fig. 2(c)) are considered, respectively. The x axis represents total thickness of Q2 which is given by its retardation and $\lambda_0 = 780$ nm. Experimental results of C_{LP} and C_{RP} (the product of $C[(\mathbb{1} \otimes \$)|\phi^+\rangle\langle\phi^+|]$ and $C(|\chi\rangle)$) are represented by red dots and blue squares, respectively. We can find that both of them overlap with each other very well, which infers that $C_{LP} = C_{RP}$. The theoretical predictions C_{LP} (solid lines) and C_{RP} (dashed lines) are calculated from equation (1) with the fitting parameters the same as the case we demonstrate the phenomenon of entanglement sudden

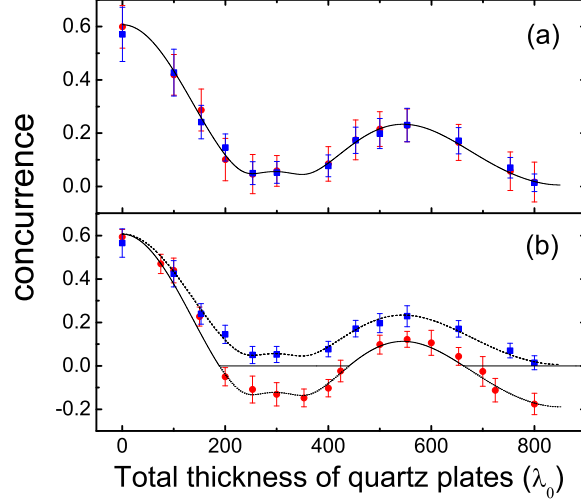


FIG. 3: (Color online). Experimental results for different mixed input states. (a) the case with inserting only $Q1=117\lambda_0$ into mode a . (b) the case with inserting both the HWP1 and $Q1=117\lambda_0$ into mode a . Red dots is the experimental results of Γ_{LM} and blue squares represent C_{RM} . The solid lines and dashed lines are the theoretical predictions of C_{LM} and C_{RM} , respectively (they completely overlap in the case of (a)). At the area of $\Gamma_{LM} \leq 0$ where the theoretical prediction is represented by dotted lines (b), the concurrence is set to 0 according to equation (1).

death [7] and they completely overlap with each other. It is also seen from fig. 2 that experimental results agree well with theoretical predictions. In our experiment, the pumping power is about 200 mW and the integration time is 6 minutes. Error bars are mainly due to the counting statistics and the uncertainties in aligning the wave plates [9].

When it comes to the case with mixed input states, the dynamics of the maximally entangled state in the channel gives the upper bound of the entanglement dynamics according to inequality (3). Fig. 3(a) shows the case with the mixed input state prepared by only inserting $Q1=117\lambda_0$ into mode a to dephase the maximally entangled state $|\phi^+\rangle$ ($\alpha^2 = \frac{1}{2}$). We can see that the experimental results agree well with the theoretical prediction and $C_{LM} = C_{RM}$. We further demonstrate the other case in which we insert both the HWP1 and $Q1=117\lambda_0$. Fig. 3(b) shows our experimental results, where the phenomenon of entanglement sudden death (C_{LM}) occurs [7]. At the area of $\Gamma_{LM} \leq 0$, the concurrence is set to 0 corresponding to equation (1). It can be seen that C_{LM} (red dots) is less than C_{RM} (blue squares) during the evolution, which is consistent with the theoretical predictions of

C_{LM} (solid line) and C_{RM} (dashed line).

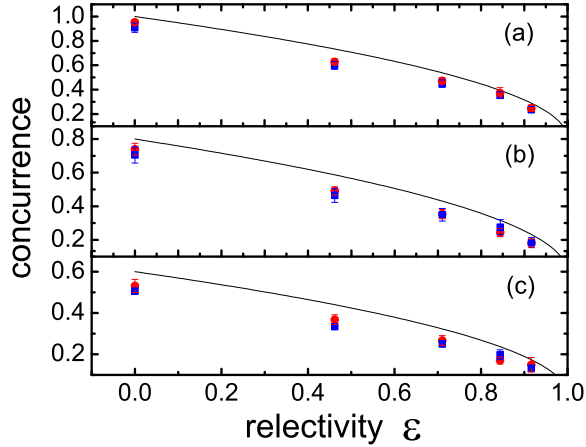


FIG. 4: (Color online). Entanglement dynamics of different pure states in the amplitude decay channel. (a) $\alpha^2 = \frac{1}{2}$. (b) $\alpha^2 = \frac{1}{5}$. (c) $\alpha^2 = \frac{1}{10}$. Red dots and blue squares represent experimental results of C_{LP} and C_{RP} , respectively. The corresponding theoretical predictions of C_{LP} (solid lines) and C_{RP} (dashed lines) completely overlap.

Now, we consider the entanglement dynamics in the amplitude decay channel, where the F-P cavity and quartz plates Q2 in the dotted pane M are replaced by the set of glass slaps tilted to the Brewster angles. By changing the number of the glass slaps, we can control the relectivity of this channel. In order not to disturb the transmitted photons, two relatively placed slaps are added or removed at the same time. The relectivity of each two slaps we measured is about 0.46. The counts of reflected photons is deduced from the difference between the transmitted vertical polarization photons without glass slaps and with glass slaps. The coincident counts of the 16 measurement bases to reconstruct the final photon-state are consisted by the corresponding transmitted and reflected parts. The transmitted counts of each measurement basis are detected by the tomography measurement setup in fig. 1, while the corresponding reflected counts is calculated as the product of the total counts of the reflected photons and the theoretical detecting probability of each measurement basis in the reflected photon-state.

Fig. 4 shows the case of the amplitude decay channel with different pure input states $|\chi\rangle$. In this experiment, the reflected photon-state is $|VH\rangle_{a,b}$. Fig. 4(a), (b) and (c) correspond to the initial state with $\alpha^2 = \frac{1}{2}$, $\frac{1}{5}$ and $\frac{1}{10}$, respectively. We can see that the experimental

results of C_{LP} (red dots) are equal to C_{RP} (blue squares). The theoretical predictions of C_{LP} (solid lines) and C_{RP} (dashed lines) are both given by $2\alpha\beta\sqrt{1-\epsilon}$. The difference between the experimental results and the corresponding theoretical predictions comes mainly from disturbance of the preparation of the initial state and the absorption of the slabs.

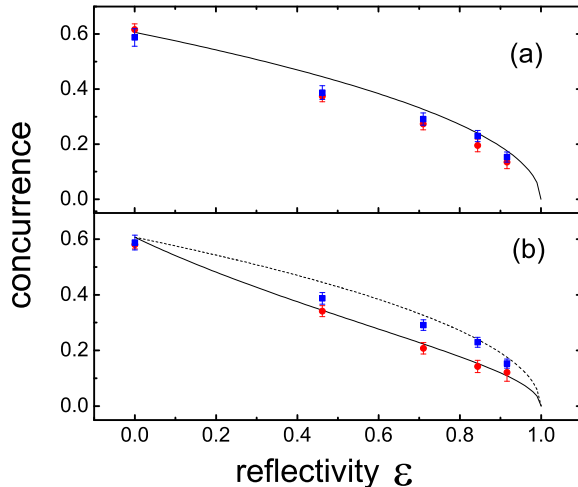


FIG. 5: (Color online). Entanglement dynamics of the amplitude decay channel for mixed input states. (a) the case with inserting only $Q1=117\lambda_0$ into mode a . (b) the case with inserting the HWP1 and $Q1=117\lambda_0$ into mode a at the same time. Experimental results are represented by red dots (C_{LM}) and blue squares (C_{RM}). Solid lines and dashed lines are the corresponding theoretical fittings of C_{LM} and C_{RM} (they completely overlap in the case of (a)).

Fig. 5 shows the experimental results of the amplitude decay channel for mixed input states. The initial mixed state in fig. 5(a) is the same as that in the case of fig. 3(a), which is prepared by inserting only $Q1=117\lambda_0$ into mode a with $\alpha^2 = \frac{1}{2}$. We find that C_{LM} (red dots) equal to C_{RM} (blue squares). The theoretical predictions of C_{LM} (solid lines) and C_{RM} (dashed lines) completely overlap and are consistent with the experimental results. Therefore, the entanglement dynamics of the inequality (3) reaches its upper bound. In another case where the initial mixed state is prepared by inserting the HWP1 and $Q1=117\lambda_0$ at the same time, we find that $C_{LM} \leq C_{RM}$ and inequality (3) holds, as shown in fig. 5(b). In this experiment, the reflected photon-state is given by $\rho_r = 1/2(|HH\rangle\langle HH| - \kappa_a^*|HH\rangle\langle VH| - \kappa_a|VH\rangle\langle HH| + |VH\rangle\langle VH|)$, where κ_a is the decoherence parameter in mode a . Experimental results agree with the corresponding theoretical prediction employing equation (1).

In conclusion, we have characterized the entanglement dynamics in quantum channels with the maximally entangled state and verified the entanglement factorization law [15]. The results provide a novel method to describe entanglement dynamics in noisy channels and would have great importance on the construction of the complex quantum network [20].

Note: After we finished this manuscript, we find that similar experimental results have been published online by Farías *et al.* [21]. They have characterized the entanglement dynamics in the amplitude decay channel, which is simulated by a modified Sagnac interferometer. In our experiment, we demonstrate the characterization both in the phase damping channel and the amplitude decay channel, which are simulated by the F-P cavity followed by quartz plates and the glass slaps with the axes tilted to the Brewster angles, respectively. What is more, the concurrence of the evolved maximally entangled state ($C[(\mathbf{1} \otimes \$)|\phi^+\rangle\langle\phi^+|]$) is calculated from the experimental form of the single channel $\$$ in their paper [21], while we measure all the quantities in equality (2) and inequality (3), and then compare the left terms and the right terms to verify the idea of characterizing the entanglement dynamics in noisy channels with the maximally entangled state.

We thank Y. X. Gong for his notification. This work was supported by National Fundamental Research Program, the Innovation funds from Chinese Academy of Sciences, National Natural Science Foundation of China (Grant No.60121503, 10874162) and Chinese Academy of Sciences International Partnership Project.

-
- [1] M. A. Nielsen and I. L. Chuang, *Quantum Computation and Quantum Information* (Cambridge University Press, Cambridge, England, 2000).
 - [2] W. H. Zurek, *Rev. Mod. Phys.* **75**, 715 (2003).
 - [3] T. Yu and J. H. Eberly, *Phys. Rev. Lett.* **93**, 140404 (2004).
 - [4] T. Yu and J. H. Eberly, *Phys. Rev. Lett.* **97**, 140403 (2006).
 - [5] M. P. Almeida *et al.*, *Science* **316**, 579 (2007).
 - [6] T. Yu and J. H. Eberly, *Science* **323**, 598 (2009).
 - [7] J.-S. Xu, *et al.*, arXiv:0903.5233.
 - [8] W. K. Wootters, *Phys. Rev. Lett.* **80**, 2245 (1998).
 - [9] D. F. V. James, P. G. Kwiat, W. J. Munro, and A. G. White, *Phys. Rev. A* **64**, 052312 (2001).

- [10] F. Mintert, A. R. R. Carvalho, M. Kuś, and A. Buchleitner, *Phys. Rep.* **415**, 207 (2005).
- [11] K. Życzkowski, P. Horodecki, M. Horodecki and R. Horodecki, *Phys. Rev. A* **65**, 012101 (2001).
- [12] A. R. R. Carvalho, F. Mintert and A. Buchleitner, *Phys. Rev. Lett.* **93**, 230501 (2004).
- [13] W. Dür and H.-J. Briegel, *Phys. Rev. Lett.* **92**, 180403 (2004).
- [14] A. R. R. Carvalho, M. Busse, O. Brodier, C. Viviescas and A. Buchleitner, *Phys. Rev. Lett.* **98**, 190501 (2007).
- [15] T. Konrad, F. de Melo, M. Tiersch, C. Kasztelan, A. Aragão and A. Buchleitner, *Nature Phys.* **4**, 99 (2008).
- [16] P. G. Kwiat, E. Waks, A. G. White, I. Appelbaum, and P. H. Eberhard, *Phys. Rev. A* **60**, R773 (1999).
- [17] J.-S. Xu, C.-F. Li, and G.-C. Guo, *Phys. Rev. A* **74**, 052311 (2006).
- [18] P. G. Kwiat, S. Barraza-Lopez, A. Stefanov, and N. Gisin, *Nature (London)* **409**, 1014 (2001).
- [19] J. Preskill, 1998 *Lecture Notes* Chapter 3 (<http://www.theory.caltech.edu/people/preskill/ph229/>).
- [20] H. J. Kimble, *Nature (London)* **453**, 1023 (2008).
- [21] O. J. Fariás, C. L. Latune, S. P. Walborn, L. Davidovich, and P. H. S. Ribeiro, *Science*, **14** May 2009 (10.1126/science.1171544).